Construction and Building Materials 470 (2025) 140522

Contents lists available at ScienceDirect

Construction and Building Materials

journal homepage: www.elsevier.com/locate/conbuildmat

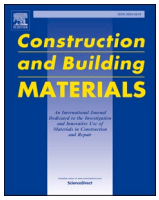

Improvement of the thermal conductivity of micronized nanocellular poly (methyl-methacrylate) (PMMA) by adding infrared blockers

Ismael Sánchez-Calderón [a,b], Félix Lizalde-Arroyo [a,*], Judith Martín-de-León [a], Miguel Ángel Rodríguez-Pérez [a,c], Victoria Bernardo [b]

[a] CellMat Laboratory, Campus Miguel Delibes, Faculty of Science, Condensed Matter Physics Department, University of Valladolid, Paseo de Belén 7, Valladolid 47011, Spain
[b] CellMat Technologies S.L, Paseo de Belén 9-A, Valladolid 47011, Spain
[c] BioEcoUVA Research Institute on Bioeconomy, University of Valladolid, Valladolid 47011, Spain

ARTICLE INFO

Keywords:
Thermal conductivity
Poly(methyl-methacrylate)
Micronized nanocellular polymer
Infrared blockers
VIP

ABSTRACT

Micronized nanocellular polymers show great potential to be used as core materials for vacuum insulation panels due to their reduced thermal conductivity under vacuum. However, as a result of their nanocellular structure, these materials are characterized by thermal radiation contributions higher than 4 mW/(m·K). This work studies how to further enhance their thermal insulation behavior by adding infrared blockers to reduce thermal radiation. Three different opacifiers (titanium(IV) oxide, graphene nanoplatelets, and silicon carbide) are used in different contents (2.5, 5, 10, 15, and 20 wt%). The obtained powders are characterized to determine the apparent density, the particle size distribution, and the thermal conductivity. The addition of infrared blockers leads to an increase in apparent density which is also related to the opacifier's particle size. For each infrared blocker, there is an optimum concentration to achieve the minimum thermal conductivity. Finally, compacted panels are produced to analyze their behavior as VIP cores by measuring thermal conductivity under vacuum conditions. A minimum thermal conductivity of 9.6 mW/(m·K) is obtained for the compacted panel containing 10 wt% of silicon carbide, a reduction of 2 mW/(m·K) regarding the sample without opacifier.

1. Introduction

Micronization of nanocellular polymers has been recently shown as a novel method to enhance the thermal insulation of nanocellular polymers[1]. Due to their discontinuous structure, these materials present lower thermal conductivity than their bulk counterparts, especially under vacuum. Thus, micronized nanocellular polymers are expected to have thermal conductivities as low as 10 mW/(m·K) at vacuum, showing a great potential to be used as a low-cost and eco-friendly core material for vacuum insulation panels (VIP)[2]. A VIP is a composite material containing a porous core covered by an envelope material in which the gas has been evacuated[3]. Thus, the heat transfer mechanisms related to the gas phase (conduction through the gas phase and coupling) are neglected[4]. The core is fabricated from an open porous material and is the inner part of the VIP, physically supporting the envelope and providing superinsulation performance. The materials usually selected as VIP cores are based on silica (fumed/precipitated silica or silica aerogel with densities around 200 kg/m^3) because, due to their nanostructure, they require a lower vacuum to fully evacuate thanks to the so-called Knudsen effect[5,6]. This effect implies that when the cell size is comparable to or smaller than the mean free path of the gas molecules (i.e. the average distance between collisions), they collide more often with the cell walls than among them, reducing the energy transfer[7]. On the one hand, thanks to the Knudsen effect, when the cell/pore size decreases the thermal conductivity at ambient pressure is reduced. On the other hand, when the pressure is reduced the thermal conductivity sharply decreases[8]. Nevertheless, the main drawbacks of nanoscale silica materials are their high price and sustainability concerns [9–13]. In this regard, the use of micronized nanocellular polymers could be a potential strategy to reduce the price and enhance the sustainability of VIP, allowing superinsulation to reach more applications.

VIPs are characterized by thermal conductivities under vacuum between 4 and 8 mW/(m·K)[14–17]. This conductivity is the sum of two main contributions once the gas phase is evacuated: the conduction through the solid phase and the radiation[8,18–20]. On the one hand,

* Corresponding author.
E-mail address: felix.lizalde@uva.es (F. Lizalde-Arroyo).

https://doi.org/10.1016/j.conbuildmat.2025.140522
Received 18 November 2024; Received in revised form 19 February 2025; Accepted 20 February 2025
Available online 28 February 2025

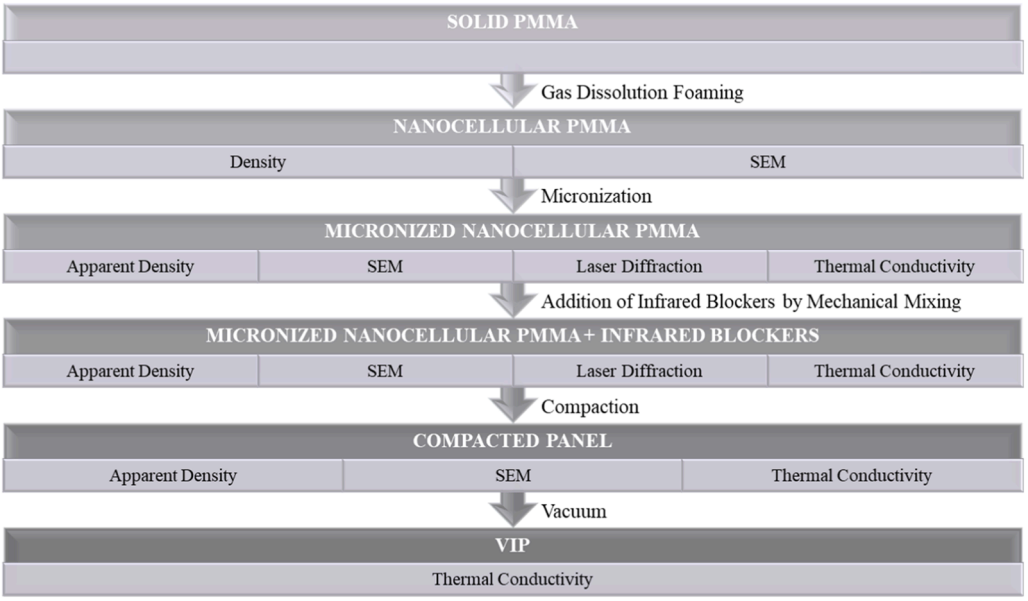

Fig. 1. Flowchart regarding sample preparation, production process, and characterization.

conduction through the solid phase depends on the density and the type of core material used. On the other hand, radiation transferred through a material depends on two main phenomena: the absorption and the scattering of thermal radiation. The absorption is determined solely by the density (amount of solid material available for absorbing radiation) and the nature of the system. Meanwhile, scattering is controlled by the size of the particles. When the pore size reduces to the nanoscale, radiation is not scattered in the structure[21]. For instance, radiation in silica-based materials can be higher than 4 mW/(m·K) at 300 K due to their high porosity (above 90 %) and nanostructure. Then, to boost the performance of the VIP core, opacifiers or infrared blockers (IR-blockers) are usually added[5,20,22–26]. An opacifier is a material that strongly absorbs or scatters infrared radiation, increasing the extinction coefficient and thus reducing heat transfer by radiation. Graphite, titanium(IV) oxide (TiO_2), and silicon carbide (SiC) are usually used [22–27]. Such materials attenuate radiation via different mechanisms; for instance, carbon-based opacifiers reduce radiation mainly by absorption, whereas TiO_2 or SiC particles both scatter and absorb radiation [22]. The addition of opacifiers (physically dispersed in the silica-based material as powder mixtures) can reduce the thermal conductivity of fumed silica core by 1–3 mW/(m·K) [22,23,25]. There is an optimum amount of opacifier that can be added since an excess can lead to higher conduction through the solid phase because opacifiers present a high thermal conductivity. For instance, Singh et al.[24] studied the radiation of fumed silica VIPs containing different contents (from 10 wt% to 40 wt %) of several opacifiers (carbon black, TiO_2, and SiC), observing a linear reduction of the thermal radiation with an increase in the proportion of opacifier. Carbon black showed the best performance, while TiO_2 showed the worst. Meanwhile, Davraz et al.[27] studied the optimum SiC content in fumed silica VIPs. Results showed that 15 wt% of SiC was the optimum. Furthermore, there is an optimum opacifier size to maximize the IR extinction which also depends on the temperature [28–30]. For instance, Wang et al.[29], reported that the optimum opacifier particle size for SiC changes from 6 to 4 μm when temperature increases from 300 to 800 K, while for carbon black the optimum particle size varies from 4 to 2 μm in the same temperature range [29].

The strategy of adding opacifiers can also be applied to reduce the radiation contribution of micronized nanocellular polymers, which can be higher than 4 mW/(m·K)[1,31]. One possibility could be adding the IR-Blockers to the polymer matrix as an additive before the foaming process, as it is done for conventional cellular polymers[26,32]. Some examples of IR-blockers used in the literature for cellular polymers are carbon-based materials (multi-walled nanotubes, carbon black nanoparticles, graphite), TiO_2, or aluminum oxide (Al_2O_3)[26,33–36]. The previously mentioned works are mainly related to the production of microcellular or conventional polymer foams since the incorporation of these additives in nanocellular polymers is not so straightforward. Firstly, the IR-Blockers need to be in the nanometric range, since they are incorporated into the solid formulation, to prevent the appearance of large cells. Furthermore, it is a challenge to achieve good dispersions of the nanometric particles without agglomeration, especially at high loads, which could also affect the foaming process[37]. The second option is dispersing the opacifier particles, as is done for fumed silica, allowing high loads without compromising the structure and foaming process of the nanocellular polymer. This second route is easy to be done with micronized nanocellular polymers and it is the strategy followed in this work.

Therefore, the present work aims to prove the concept of preparing powder mixtures of micronized nanocellular PMMA and infrared blockers to enhance thermal insulation. The materials are studied to be used as core materials for VIPs. Three different types of opacifiers are used in several contents. The obtained powders are characterized to determine the apparent density, the particle size distribution, and the thermal conductivity. Finally, compacted panels are produced and their thermal conductivity is measured at ambient pressure and under different vacuum pressures. The results obtained would pave the way for the use of these materials as low-cost VIP core materials.

2. Experimental

2.1. Materials and sample preparation

PLEXIGLAS® 7 H (Röhm GmbH) was the PMMA grade used to produce the nanocellular material by gas dissolution foaming. Details of the PMMA, the gas dissolution foaming equipment used and the two-step foaming process can be found elsewhere[38]. In particular, the saturation conditions were 31 MPa and 40 °C, while the foaming parameters were 90 °C and 5 min. Fig. 1 shows a flowchart regarding sample preparation, the production process followed, and the characterization techniques used.

The main features of the bulk nanocellular material were: 100 kg/m^3 of density, 800 nm of cell size, and 0.5 of normalized standard deviation

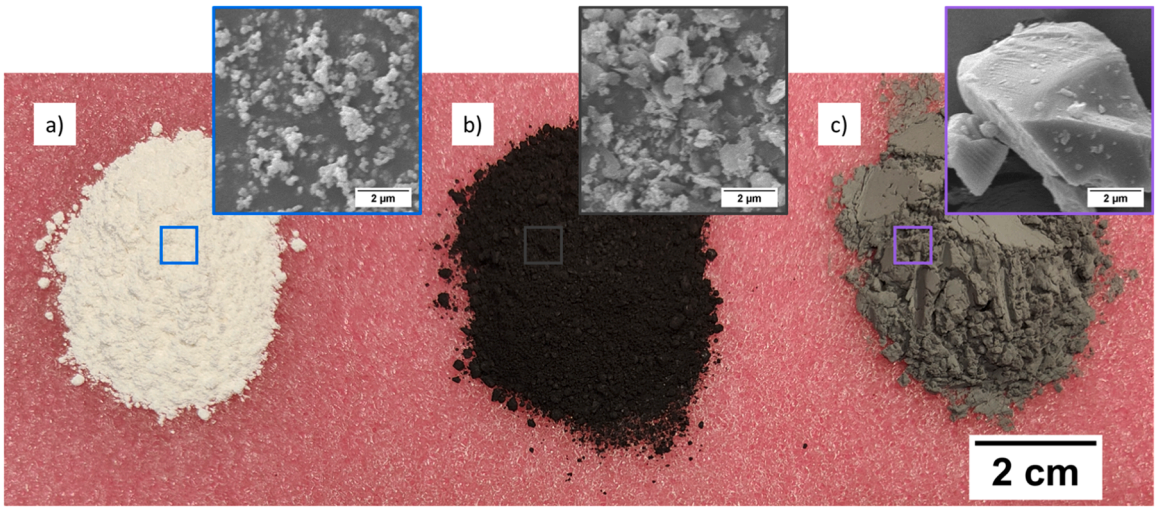

Fig. 2. Photograph and SEM micrographs of the opacifiers used in this work: a) TiO_2, b) GnP, and c) SiC.

Table 1
Particle size of the opacifiers used in this work (from the technical datasheets).

IR-Blocker	Particle Size
TiO_2	100–150 nm of diameter
GnP	7 µm of lateral size 2–3 nm of thickness
SiC	5 µm of diameter

of the cell size distribution. Then, the material was micronized using a rotor beater mill SR 300 (Retsch) (Fig. 1). After the milling process, the resultant material was a homogeneous powder characterized by an apparent density of 80 kg/m^3, micrometric particles with a mean particle size of 146 µm (obtained by laser diffraction), 100 % of open cell content, and a similar cell size to the bulk nanocellular material (800 nm). Details of the procedure to produce and characterize the micronized nanocellular material can be found in our previous works[1, 2].

To study the effect of the addition of IR-Blockers, three different types of opacifiers were added and physically mixed with the low-density nanocellular powder in different contents (2.5, 5, 10, 15, and 20 wt%) (Fig. 1). The materials were mixed manually until the blend was observed to be homogeneous. The IR-Blockers used in this work were: titanium dioxide (TiO_2) supplied by Riedel-de Haën (product code: 14027), graphite nanoplatelets (GnP) PLAT7 provided by Avanzare, and silicon carbide (SiC) F1000 supplied by Navarro SiC. Fig. 2 shows the appearance of the powders and their particles visualized with scanning electron microscopy (SEM). TiO_2 is a white powder of spherical particles, GnP is a black powder of lamellar particles, and SiC is a gray powder of polyhedral particles. Table 1 summarizes the particle size of the opacifiers (obtained from the technical datasheets). The apparent density of the IR-Blockers, measured according to ISO 60[39], is: 640 kg/m^3 for the TiO_2 nanoparticles, 700 kg/m^3 for the SiC particles, and 390 kg/m^3 for the GnP.

Finally, the pure sample and the samples containing 10 wt% of each IR-Blocker were compacted to prepare panels using a hot plate hydraulic press with accurate control provided by Talleres Remtex (Barcelona, Spain) (Fig. 1). First, the micronized samples were dried at 60 °C for 30 min in a forced-air high-temperature oven (model 2001405, JP Selecta). Second, the necessary amount of sample was weighed and placed inside a mold with final dimensions of 120 × 120 × 15 mm^3. The target apparent density of the compacted samples is 147 kg/m^3 for the pure sample and 162 kg/m^3 for the samples containing an additional amount of 10 wt% IR-Blocker. The density was selected to obtain self-standing panels and to properly analyze the effect of the addition of opacifiers to the pure sample, keeping the same amount of pure nanocellular polymer in all the samples. Afterward, the mold is placed on the press under 20 tons at 80 ºC for 30 min. Finally, the sample is removed from the mold obtaining a compacted panel.

Regarding VIP production (Fig. 1), a set-up consisting of a vacuum pump (RV3, Edwards), a vacuum controller (VacuuSelect + VV-B15C electrovalve + Pirani VacuuWiew extend sensor, Vacuubrand), a vacuum valve (VAC VALVE 425, Matva), and an envelope (Pack-lab) were used. First, the material is wrapped in fleece and introduced in a two layers envelope with a composition of metalized poly(ethylene terephthalate) (PET) (thickness of 12 µm) and polyethylene (PE) (sealant, 80 µm in thickness). The envelope is connected to the vacuum devices (pump and vacuum controller) through a vacuum valve and different accessories. Once the wrapped material is inside the envelope the borders of the bag are sealed. Finally, the pump is connected to produce the VIP, and the vacuum inside is controlled with the vacuum set-up.

2.2. Characterization

2.2.1. Density

The apparent density of the powder mixtures was obtained according to ISO 60[39]. Meanwhile, the apparent density of the compacted panels was obtained according to UNE-EN 1602[40].

2.2.2. Surface morphology (SEM)

A Scanning Electron Microscope (FlexSEM 1000 VP-SEM) was used to visualize the IR-blockers and the surface of the micrometric nanocellular particles with and without opacifiers. Prior visualization the samples were coated with gold using a sputter coater (model SCD 005, Balzers Union).

2.2.3. Volume particle size distribution (laser diffraction)

Laser diffraction measurements were performed to study the particle size distribution of the micronized nanocellular polymer and the mixtures containing 10 wt% content of opacifier. Experiments were carried out at CENIEH (Burgos, Spain) using a LS13 320 Particle Size Analyzer (Beckman Coulter). Details about the procedure can be found in [1].

2.2.4. Thermal conductivity measurements (Heat Flow Meter)

Thermal conductivity measurements were performed using a thermal heat flow meter model FOX 200 (TA Instruments / LaserComp, Inc.). This equipment measures according to ASTM C518 and ISO 8301[41,

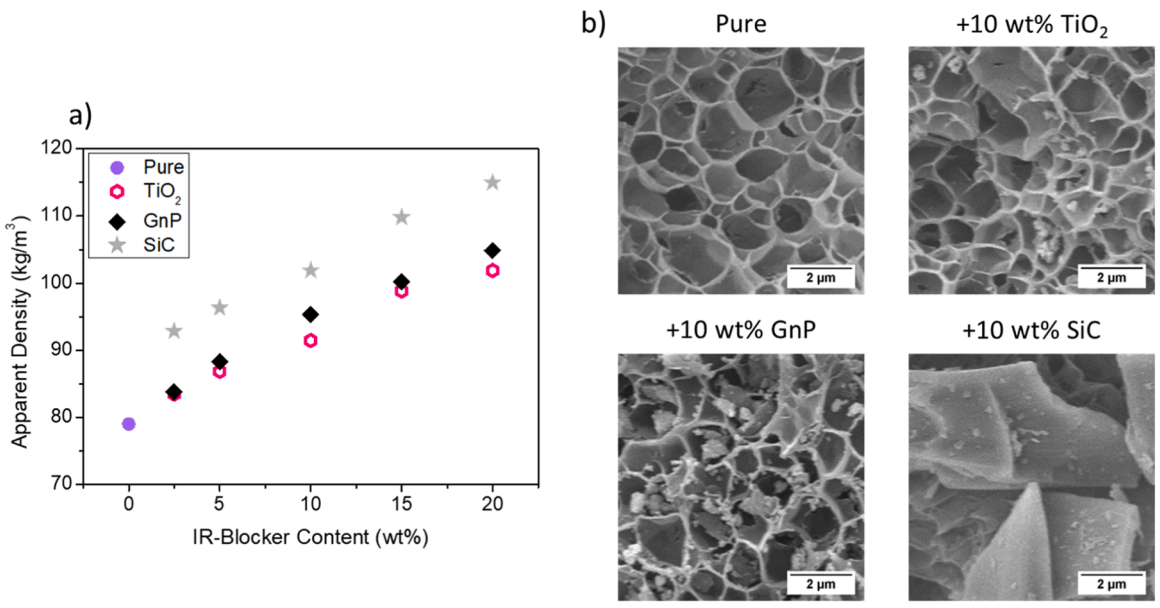

Fig. 3. a) Apparent density of the samples as a function of the type and content of IR-Blocker and b) SEM micrographs of the reference sample (pure) and the samples with 10 wt% of each IR-Blocker.

42] (steady-state conditions) in a range between 5 and 350 mW/(m·K) with a relative accuracy of ± 1 %[2]. Therefore for a measurement of 33 mW/(m·K) the uncertainty is 0.33 mW/(m·K), while for a measurement of 10 mW/(m·K) the uncertainty is 0.1 mW/(m·K)[43]. For the measurements, the sample was placed between the two plates using the same procedure as in our previous works[1,2], promoting a temperature gradient (ΔT) of 20 ºC through the material thickness. It is important to note that the samples have larger dimensions than the FOX 200 heat flux transducers (120 × 120 mm^2 vs 75 × 75 mm^2).

On the one hand, for the measurement of the thermal conductivity of the free powders, a polyurethane foam mask (with a size of 200 × 200 × 14 mm^3) with a hole of 120 × 120 mm^2 in the center was used to hold the free powder[1]. An aluminum foil placed on the bottom of the mask was used to avoid the loss of powder. These measurements were performed at ambient pressure and at four different mean temperatures 10, 20, 30, and 40 ºC (i.e., for the measurement at 10 ºC, the temperature goes from 0 ºC in the upper isothermal plate to 20 ºC in the lower one).

On the other hand, the thermal conductivity of the compacted samples was measured at 10 ºC of mean temperature at ambient pressure and under vacuum (600, 300, 200, 100, 60, 30, 10, 6, 3, and 0.02 mbar) [2]. Note that 1 bar = 1000 mbar = 100,000 Pa. For the measurement, the material wrapped inside the envelope is connected through a vacuum valve to the vacuum set-up, allowing the control of the inner pressure from 0.001 to 1100 mbar. The accuracy of the vacuum measurement is ± 15 % in the range of 0.001–5 mbar and for pressures from 5 to 1100 mbar the accuracy is ± 3 mbar. For instance, for a vacuum measurement of 1 mbar the uncertainty is 0.15 mbar, meanwhile at 200 mbar the uncertainty 3 mbar. The time between reaching the vacuum pressure and the start of the thermal conductivity measurement is 3 hours.

3. Results and discussion

3.1. Effect of the addition of IR-blockers on the apparent density and the surface of the micrometric particles

The powder mixtures obtained are homogeneous, with the opacifiers

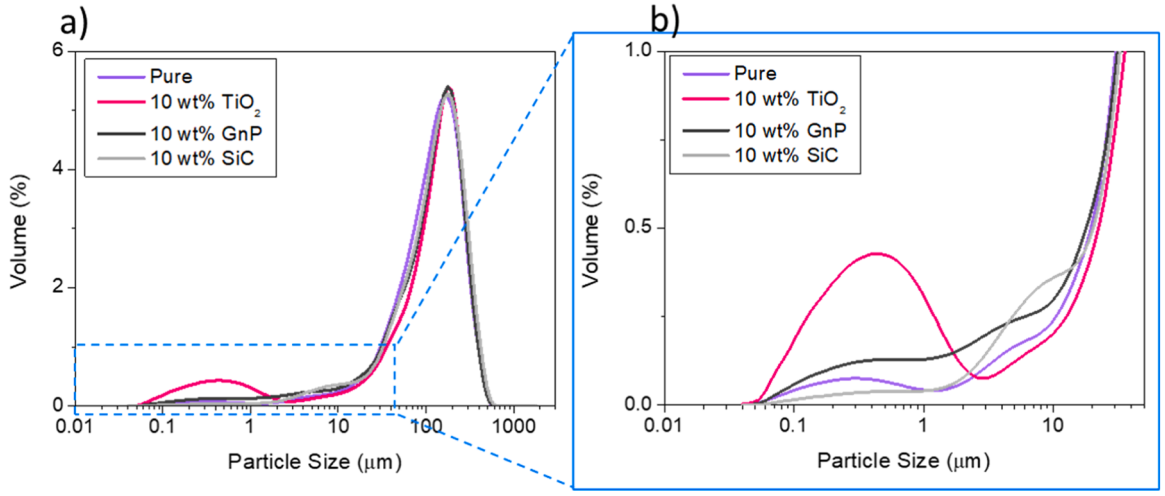

Fig. 4. Dynamic laser diffraction %volume particle size distributions of the reference sample (pure) and the samples containing 10 wt% of each IR-blocker: a) full distribution and b) zoom in the region < 50 µm.

Table 2
Mean particle size (*D*) and normalized standard deviation of the particle size distribution (*SD/D*) results of the reference sample (pure) and the samples containing 10 wt% of IR-blocker obtained by laser diffraction.

IR-Blocker	*D* (μm)	*SD/D* (μm)
Pure	146	0.68
+ 10 wt% TiO_2	143	0.75
+ 10 wt% GnP	144	0.71
+ 10 wt% SiC	153	0.70

well-dispersed through the micronized nanocellular PMMA. Fig. 3 shows the density of the powder blends (Fig. 3**a**) and the surface of the micrometric nanocellular PMMA particles with 10 wt% of each IR-blocker (Fig. 3**b**). It is observed that as the IR-Blocker content increases, the apparent density of the resultant powder mixture increases because the opacifier is characterized by a much higher density (Fig. 3**a**). In particular, TiO_2 nanoparticles and GnP are placed inside the exposed superficial cells (the diameter of the cells is 800 nm) due to their reduced size (Fig. 3**b**). Thus, despite the higher apparent density of the TiO_2 nanoparticles in comparison with the GnP, the mixtures containing TiO_2 and GnP show a similar density trend. However, the apparent density of the GnP blends is slightly higher probably due to the higher particle size of the GnP (some particles may not enter inside the nanocells) which could be affecting the packaging. This packaging fact is observed in the SiC mixtures, which present much higher apparent densities, even for low contents of SiC. Note that the SiC particles (size 5 μm) are too large to enter the nanometric structure (Fig. 3**b**). For instance, for an IR-Blocker content of 10 wt%, the apparent density goes from 91 kg/m^3 (TiO_2) to 102 kg/m^3 (SiC). In comparison to the pure polymer, this represents an increase of 15 % and 29 %, respectively. Therefore, the change in the packaging affects the blend density, leading to higher densities when the particles are larger than the pore size. Therefore, the different behaviors can be related to the opacifier's particle size (Fig. 4 and Table 1) and how it is distributed on the nanocellular PMMA micrometric particles (Fig. 3**b**).

Laser diffraction measurements were conducted to study the size of the particles in the blends. Due to the measurement procedure (dispersion of the powder in EtOH), the opacifier particles leave the nanocellular PMMA surface being dispersed together with the micronized nanocellular PMMA particles in the solvent. Fig. 4 shows the particle size distribution of the reference sample (pure), and the powder blends containing 10 wt% of each opacifier. All the samples present a similar mean particle size (*D*) to the original size of the PMMA micrometric particles (146 μm) (Table 2). However, the normalized standard deviation of the particle size (*SD/D*) of the samples containing opacifiers is slightly higher since the blend contains also smaller particles. In the pure polymer, there is a small fraction of particles with sizes below 10 μm (Fig. 4**b**). GnP increases the fraction of these small particles. Then, the

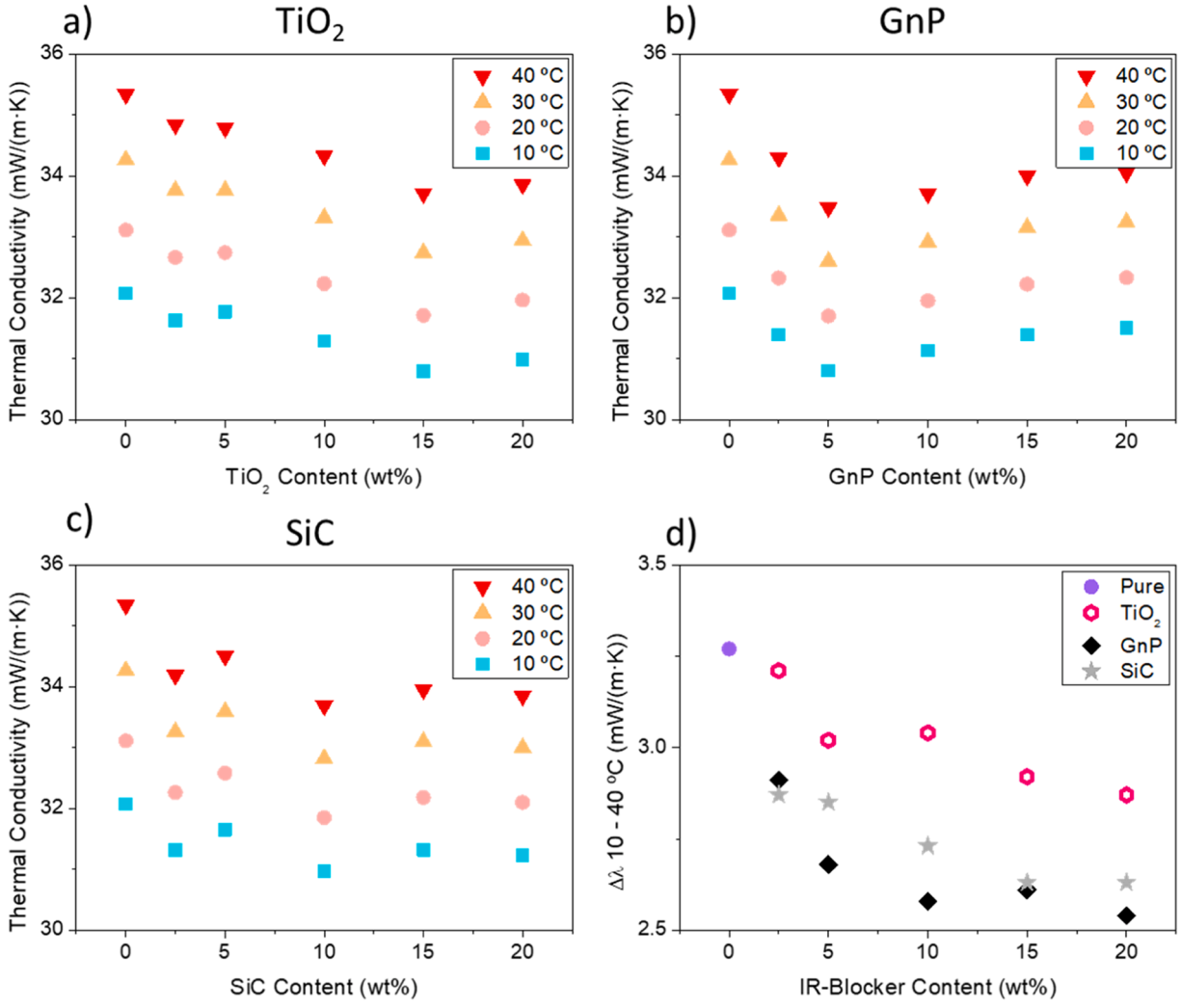

Fig. 5. Thermal conductivity as a function of the IR-Blocker content at different temperatures for TiO_2 (a), GnP (b), and SiC (c); and thermal conductivity gap (d) between the measurements performed at 10 ºC and 40 ºC as a function of the type and content of each IR-Blocker.

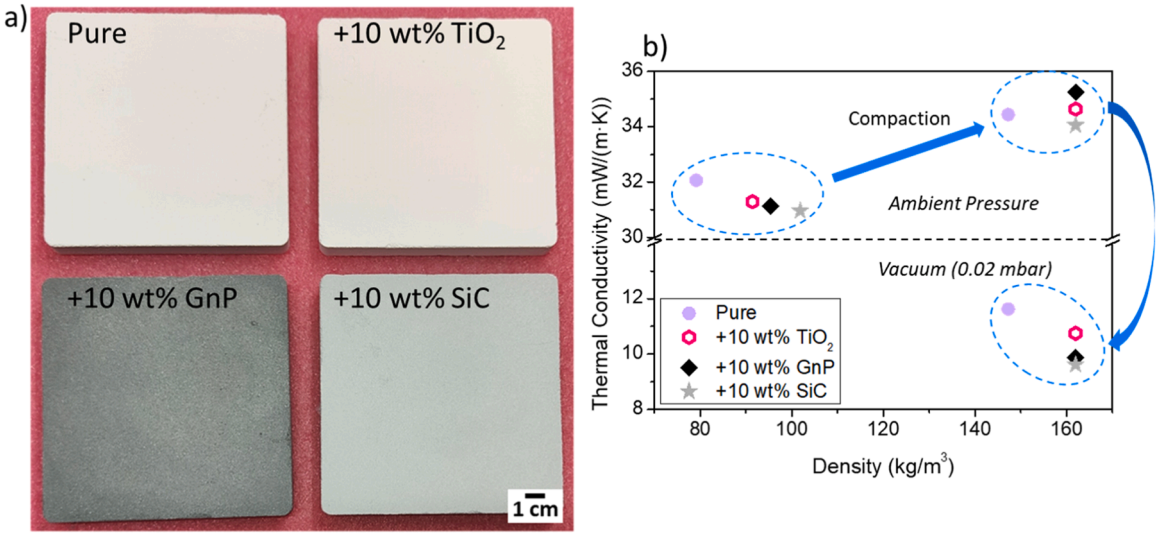

Fig. 6. a) Photograph of the compacted panels produced in this work. b) Thermal conductivity at 10 ºC of the reference sample and the samples with 10 wt% of opacifiers as a function of the density of the compacted samples produced in this work at ambient pressure and at vacuum (0.02).

presence of TiO_2 particles generates an extra peak at around 400 nm, corresponding to TiO_2 particles and particle aggregates. Meanwhile, SiC particles generate a shoulder around 5 μm, which is the size of these particles.

3.2. Effect of the addition of IR-blockers on the thermal conductivity

3.2.1. Powder mixtures

Figs. 5**a**, 5**b**, and 5**c** show the thermal conductivity as a function of the IR-Blocker content at different temperatures (10, 20, 30, and 40 ºC) for TiO_2, GnP, and SiC, respectively. The reference sample (pure) is found at the point of 0 wt% of IR-blocker in every graph. In general, as the amount of opacifier in the mixture increases the thermal conductivity is reduced until it reaches a minimum, then the thermal conductivity rises again. The thermal conductivity of a porous powder material such as these blends depends on four mechanisms: conduction through the cells in the nanocellular powder, conduction through the solid phase, coupling between the solid particles and the gas surrounding them, and radiation[31]. When adding IR-Blockers there is a compromise between radiation reduction and conduction through the solid phase rise. As the amount of opacifiers increases, the highly conductive particles are more in touch with one another, increasing the heat transfer by conduction through the solid opacifier particles. This explains the presence of the minimum observed in the different systems: for low IR-blocker contents, radiation is reduced, but at high concentrations, there is higher conduction through the solid phase. On the other hand, as the temperature increases, the thermal conductivity increases. The minimum thermal conductivies obtained are 30.8 mW/(m·K) for 15 wt% TiO_2 (99 kg/m^3), 30.8 mW/(m·K) for 5 wt % GnP (88 kg/m^3), and 31.0 mW/(m·K) for 10 wt% SiC (102 kg/m^3). Thus, the IR-blockers used in this work lead to reductions of thermal conductivity of around 1.2 mW/(m·K) regarding the reference sample (pure) at ambient pressure. However, the optimum amount of opacifier varies, meaning different infrared radiation-blocking behaviors. The IR-blocker leading to the minimum thermal conductivity at lower content (GnP in this case) is the one with the highest infrared radiation blocking behavior.

Fig. 5**d** shows the thermal conductivity gap ($\Delta\lambda$), defined as the difference between the thermal conductivity measurements performed at 10 ºC and 40 ºC. This is an interesting parameter since the radiation term depends on the temperature cube[44,45], whereas the rest of the parameters (conduction through the solid phase, conduction through the gas phase, and coupling) depend linearly on temperature[31]. Therefore, slight variations in the temperature significantly affect the radiation contribution, so the thermal conductivity gap is related mostly to radiation. The reduction of $\Delta\lambda$ when the opacifier content increases mean that indeed the IR-blockers are decreasing the radiation contribution. It is observed that the gap is lower when using GnP followed closely by SiC and finally TiO_2. From these measurements, we can distinguish between the effects on the radiation and conduction through the solid phase terms. For TiO_2, $\Delta\lambda$ reduces continuously for all the concentrations tested up to 20 wt%, so there is a radiation reduction in all the range. However, the optimum TiO_2 content was 15 wt% and the conductivity was measured to increase later on. Then, for 20 wt% of TiO_2, there is an increase in the solid conduction that compensates the reduction in the radiation contribution. Meanwhile, for GnP, $\Delta\lambda$ reduces until 10 wt% and then remains constant. The optimum GnP content was 5 wt% meaning that for higher contents there is an increase in the solid conduction that compensates the reduction in the radiation contribution. Also, it is observed that $\Delta\lambda$ at 5 wt% for GnP is lower than in the other systems at the different concentrations, meaning that, as previously commented, GnP has higher infrared radiation-blocking behavior than SiC and TiO_2. Finally, for SiC, $\Delta\lambda$ reduces until 15 wt% and then maintains constant. Since the optimum SiC content was 10 wt%, for higher contents there is an increase in the solid conduction that compensates for the reduction in the radiation contribution.

These results prove that adding IR-blockers can help to reduce the conductivity of the micronized nanocellular PMMA powder in 1.2 mW/(m·K) (3.7 %). In the next section, compacted panels are produced and their thermal conductivity is studied at ambient pressure and under vacuum.

3.2.2. Compacted panels

The samples containing 10 wt% of opacifiers were compacted to the same final density (162 kg/m^3), obtaining self-standing panels of dimensions 120 × 120 × 15 mm^3 (Fig. 6**a**). The reference sample (pure) was also compacted to a final density of 147 kg/m^3 for sake of comparison (same amount of PMMA as the opacified samples). The results of the thermal conductivity as a function of the density for the measurements performed at 10 ºC under ambient pressure and ultimate vacuum (0.02 mbar) are shown in Fig. 6**b**. Due to the compaction process, the thermal conductivity increases between 2 and 4 mW/(m·K) with respect to the powder since the compacted samples are characterized by a higher amount of material per unit volume (higher conduction through the solid phase). Regarding the compacted samples at ambient pressure, all the samples present similar thermal conductivities in the range of

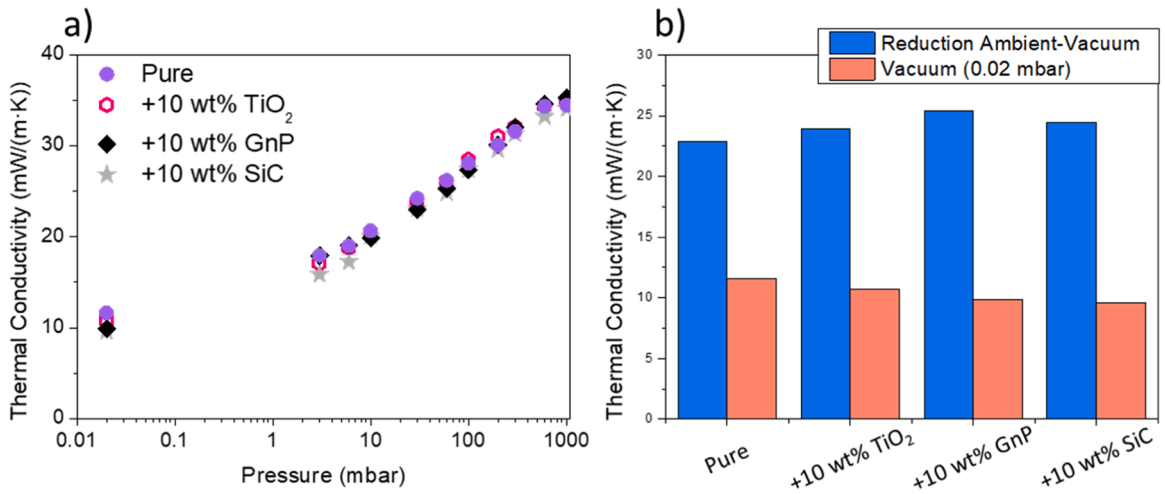

Fig. 7. a) Thermal conductivity at 10 °C of the compacted panels produced in this work at different vacuum pressures. b) Thermal conductivity at maximum vacuum (at 10 °C and 0.02 mbar) and thermal conductivity reduction between ambient and vacuum conditions (at 10°C) of the compacted panels produced in this work.

34.0–35.3 mW/(m·K) despite the higher density of the samples containing opacifiers. Note that in this range, the measurement uncertainty is around 0.35 mW/(m·K). Therefore, since, in principle, all the materials contain the same amount of micronized nanocellular PMMA, it can be stated that the percolation between the particles is minimal.

When vacuuming, the thermal conductivity is sharply reduced (Fig. 7). This is because, in systems based on contact particles, a coupling effect between the particles and the gas surrounding the particles arises [4,46–48]. When the sample is fully evacuated it is negligible due to the lack of gas molecules, however, it can represent around 55 % of the total thermal conductivity at ambient pressure[31]. In addition, the gas inside the cells of the micronized polymer is also removed. Thus, at maximum vacuum, the only heat transfer mechanisms affecting the system are the conduction through the solid phase and the radiation. As shown in Fig. 7**b**, the difference between the measurements under ambient and vacuum conditions was more significant in the samples with IR-blockers. The reason is that the coupling effect contribution depends on the density (the higher density, the higher coupling)[4,31, 49]. Also, differences in the thermal conductivity reduction when vacuuming between the compacted panels containing opacifiers may be due to the influence of each type of particle on the coupling mechanism. All the samples with opacifiers present lower thermal conductivity than the reference (pure) compacted panel (11.6 (mW/(m·K)) (Fig. 7**b**). Note that in the range of 10 mW/(m·K), the measurement uncertainty is around 0.1 mW/(m·K). For instance, the thermal conductivity of the TiO_2 sample is 10.8 mW/(m·K), almost 1 mW/(m·K) lower than the reference despite the higher density. Meanwhile, GnP and SiC samples present the lowest thermal conductivities (9.9 mW/(m·K) and 9.6 mW/(m·K) respectively), 2 mW/(m·K) lower than the thermal conductivity of the reference (pure) compacted panel.

These last results confirm that adding IR-blockers helps to reduce the thermal conductivity of the compacted panels based on micronized nanocellular PMMA, boosting their performance as VIP core material. Thermal conductivities below 10 mW/(m·K) can be obtained under vacuum. The findings of this work are promising and pave the way for further research and improvement, such as the analysis of the mixing effect by using different techniques and parameters, the fine-tuning of the content of the opacifier, and the determination of the optimum density of the compacted panel.

4. Conclusions

In this work, the effect of the addition of infrared blockers to micronized nanocellular PMMA has been analyzed. Three different opacifiers (TiO_2, GnP, and SiC) have been added to the reference (pure) sample in different contents (2.5, 5, 10, 15, and 20 wt%). On the one hand, regarding the powder mixtures, as the amount of IR-Blocker increases the density increases. Depending on the size of the opacifier particles the packaging changes, affecting the final density. Furthermore, the addition of opacifiers reduces thermal conductivity. For each IR-Blocker there is an optimum amount that leads to the minimum of thermal conductivity (a compromise between reducing the radiation and increasing the conduction through the solid phase). On the other hand, regarding the compacted panels, when compacting the thermal conductivity increases because of the density increase (higher conduction through the solid phase). When extracting the gas phase under vacuum, the thermal conductivity sharply decreases to 9.6 mW/(m·K) for the sample containing 10 wt% of SiC, which is 2 mW/(m·K) lower than the thermal conductivity of the reference (pure) compacted panel despite the higher density of the sample with SiC. These results confirm these materials as potential candidates to be used as alternative, low-cost, and eco-friendly VIP cores.

CRediT authorship contribution statement

Bernardo Victoria: Writing – review & editing, Supervision, Conceptualization. **Rodríguez-Pérez Miguel Angel:** Writing – review & editing, Supervision, Funding acquisition, Conceptualization. **Martin-de-León Judith:** Supervision, Conceptualization. **Lizalde Arroyo Félix:** Investigation. **Sánchez-Calderón Ismael:** Writing – original draft, Methodology, Investigation, Formal analysis, Conceptualization.

Declaration of Competing Interest

The authors declare that they have no known competing financial interests or personal relationships that could have appeared to influence the work reported in this paper.

Acknowledgments

Financial support from the Junta of Castile and Leon grant (I. Sánchez-Calderón and VA202P20) is gratefully acknowledged. Financial assistance from the Spanish Ministry of Science, Innovation, and Universities (PID2021–126046OB-C22, PDC2022–133391-I00, TED2021–129419B-C22 and PTQ2019–010560 (Victoria Bernardo)) is gratefully acknowledged. Financial assistance from the European Regional Development Fund of the European Union and the of Castile and Leon ((ICE): R&D PROJECTS IN SMEs: PAVIPEX. 04/18/VA/008

and M-ERA.NET PROJECT: FICACEL. 11/20/VA/0001) is gratefully acknowledged. This work was supported by the Regional Government of Castilla y León (Junta de Castilla y León) and by the Ministry of Science and Innovation MICIN and the European Union NextGenerationEU/PRTR. We would also like to thank Leticia Miguens (CENIEH) for the laser diffraction measurements.

Data availability

Data will be made available on request.

References

[1] I. Sánchez-Calderón, V. Bernardo, D. Cuadra-Rodríguez, J. Martín-de-León, M.Á. Rodríguez-Pérez, Micronization as a solution for enhancing the thermal insulation of nanocellular poly(methyl-methacrylate) (PMMA), Polymers 261 (2022) 125397, https://doi.org/10.1016/j.polymer.2022.125397.
[2] I. Sánchez-Calderón, V. Bernardo, F. Lizalde-Arroyo, J. Martín-de-León, M.Á. Rodríguez-Pérez, Development of new vacuum insulation core panels using micronized nanocellular poly(methyl-methacrylate) (PMMA), Appl. Mater. Today 41 (2024) 102483, https://doi.org/10.1016/j.apmt.2024.102483.
[3] D. Božiček, J. Peterková, J. Zach, M. Košir, Vacuum insulation panels: An overview of research literature with an emphasis on environmental and economic studies for building applications, Renew. Sustain. Energy Rev. 189 (2024), https://doi.org/10.1016/j.rser.2023.113849.
[4] S. Sonnick, M. Meier, J. Ross-Jones, L. Erlbeck, I. Medina, H. Nirschl, M. Rädle, Correlation of pore size distribution with thermal conductivity of precipitated silica and experimental determination of the coupling effect, Appl. Therm. Eng. 150 (2019) 1037–1045, https://doi.org/10.1016/j.applthermaleng.2019.01.074.
[5] S.E. Kalnæs, B.P. Jelle, Vacuum insulation panel products: a state-of-the-art review and future research pathways, Appl. Energy 116 (2014) 355–375, https://doi.org/10.1016/j.apenergy.2013.11.032.
[6] J. Fricke, H. Schwab, U. Heinemann, Vacuum insulation panels – exciting thermal properties and most challenging applications, Int. J. Thermophys. 27 (2006) 1123–1139, https://doi.org/10.1007/s10765-006-0106-6.
[7] Z.-Y. Li, C.-Y. Zhu, X.-P. Zhao, A theoretical and numerical study on the gas-contributed thermal conductivity in aerogel, Int. J. Heat. Mass Transf. 108 (2017) 1982–1990, https://doi.org/10.1016/j.ijheatmasstransfer.2017.01.051.
[8] S.S. Shrestha, J. Tiwari, A. Rai, D.E. Hun, D. Howard, A.O. Desjarlais, M. Francoeur, T. Feng, Solid and gas thermal conductivity models improvement and validation in various porous insulation materials, Int. J. Therm. Sci. 187 (2023) 108164, https://doi.org/10.1016/j.ijthermalsci.2023.108164.
[9] F.A. Almeida, J. Corker, N. Ferreira, M.A. Neto, M. Fan, H. Beyrichen, R. Caps, Alternative low cost based core systems for vacuum insulation panels, Cienc. e Tecnol. Dos. Mater. 29 (2017) e151–e156, https://doi.org/10.1016/j.ctmat.2016.10.002.
[10] B. Chang, L. Zhong, M. Akinc, Low cost composites for vacuum insulation core material, Vacuum 131 (2016) 120–126, https://doi.org/10.1016/j.vacuum.2016.05.027.
[11] J. Corker, I. Marques, S. Resalati, T. Okoroafor, A. Maalouf, Z. Fu, M. Fan, Al-rich industrial waste as new alternative of fumed silica for the manufacture of vacuum insulation panels for building energy conservation, J. Clean. Prod. 415 (2023) 137854, https://doi.org/10.1016/j.jclepro.2023.137854.
[12] Q. Sun, J. Xu, C. Lu, S. Zhu, G. Lin, M. Fan, J. Li, K. Chen, Green and sustainable kapok fibre as novel core materials for vacuum insulations panels, Appl. Energy 347 (2023) 121394, https://doi.org/10.1016/j.apenergy.2023.121394.
[13] T. Raad, S. Verma, H. Singh, Tree waste based advanced thermal insulation – vacuum insulation panels – For application at up to 70 °C, Int. J. Therm. Sci. 200 (2024) 108971, https://doi.org/10.1016/j.ijthermalsci.2024.108971.
[14] W. Villasmil, L.J. Fischer, J. Worlitschek, A review and evaluation of thermal insulation materials and methods for thermal energy storage systems, Renew. Sustain. Energy Rev. 103 (2019) 71–84, https://doi.org/10.1016/j.rser.2018.12.040.
[15] M. Casini, Smart Buildings, 2016th ed., Elsevier, 2016. https://doi.org/10.1016/C2015-0-00182-4.
[16] S. Schiavoni, F. D'Alessandro, F. Bianchi, F. Asdrubali, Insulation materials for the building sector: a review and comparative analysis, Renew. Sustain. Energy Rev. 62 (2016) 988–1011, https://doi.org/10.1016/j.rser.2016.05.045.
[17] M. Casini, Advanced construction materials, in: Constr. 4.0, Elsevier, 2022: pp. 337–404. https://doi.org/10.1016/B978-0-12-821797-9.00005-2.
[18] M.R. Jalali, D. Kaushik, S. Verma, H. Singh, A coupled model of finite element method and Mie theory for heat transfer inside expanded perlite vacuum insulation panels (VIPs) at high temperatures, Int. J. Heat. Mass Transf. 219 (2024) 124885, https://doi.org/10.1016/j.ijheatmasstransfer.2023.124885.
[19] S. Sonnick, H. Nirschl, M. Rädle, Silica-based core materials for thermal superinsulations in various applications, Int. J. Energy Res. 46 (2022) 18394–18409, https://doi.org/10.1002/er.8453.
[20] D. Kaushik, H. Singh, S.A. Tassou, Vacuum insulation panels for high-temperature applications – design principles, challenges and pathways, Therm. Sci. Eng. Prog. 48 (2024) 102415, https://doi.org/10.1016/j.tsep.2024.102415.
[21] L.W. Hrubesh, R.W. Pekala, Thermal properties of organic and inorganic aerogels, J. Mater. Res. 9 (1994) 731–738, https://doi.org/10.1557/JMR.1994.0731.
[22] R. Caps, J. Fricke, Thermal conductivity of opacified powder filler materials for vacuum insulations, Int. J. Thermophys. 21 (2000) 445–452, https://doi.org/10.1023/A:1006691731253.
[23] M. Davraz, M. Koru, H.C. Bayrakçi, Y. Yusufoğlu, O. Ipek, The effect of opacifier properties on thermal conductivity of vacuum insulation panel with fumed silica, J. Therm. Anal. Calorim. 142 (2020) 1377–1386, https://doi.org/10.1007/s10973-020-09277-8.
[24] H. Singh, M. Geisler, F. Menzel, Experimental investigations into thermal transport phenomena in vacuum insulation panels (VIPs) using fumed silica cores, Energy Build. 107 (2015) 76–83, https://doi.org/10.1016/j.enbuild.2015.08.004.
[25] M. Davraz, H.C. Bayrakci, Performance properties of vacuum insulation panels produced with various filling materials, Sci. Eng. Compos. Mater. 21 (2014) 521–527, https://doi.org/10.1515/secm-2013-0162.
[26] F. Almeida, H. Beyrichen, N. Dodamani, R. Caps, A. Müller, R. Oberhoffer, Thermal conductivity analysis of a new sub-micron sized polystyrene foam, J. Cell. Plast. 57 (2021) 493–515, https://doi.org/10.1177/0021955X20943101.
[27] M. Davraz, H.C. Bayrakçi, Y. Yusufoğlu, The effect of fiber, opacifier ratios and compression pressure on the thermal conductivity of fumed silica based vacuum insulation panels, Arab. J. Sci. Eng. 41 (2016) 4263–4272, https://doi.org/10.1007/s13369-016-2031-8.
[28] V. Napp, R. Caps, H. Ebert, Optimization of the thermal radiation extinction of silicon carbide in a silica powder matrix, J. Therm. Anal. Calorim. 56 (1999) 77–85, https://doi.org/10.1023/A:1010131324100.
[29] X.D. Wang, D. Sun, Y.Y. Duan, Z.J. Hu, Radiative characteristics of opacifier-loaded silica aerogel composites, J. Non Cryst. Solids 375 (2013) 31–39, https://doi.org/10.1016/j.jnoncrysol.2013.04.058.
[30] C.-Y. Zhu, Z.-Y. Li, H.-Q. Pang, N. Pan, Design and optimization of core/shell structures as highly efficient opacifiers for silica aerogels as high-temperature thermal insulation, Int. J. Therm. Sci. 133 (2018) 206–215, https://doi.org/10.1016/j.ijthermalsci.2018.07.032.
[31] I. Sánchez-Calderón, F. Lizalde-Arroyo, J. Martín-de-León, M.Á. Rodríguez-Pérez, V. Bernardo, Coupling effect in compacted panels based on micronized nanocellular polymers: modeling of the thermal conductivity, Int. Commun. Heat. Mass Transf. 162 (2025) 108582, https://doi.org/10.1016/j.icheatmasstransfer.2025.108582.
[32] P. Buahom, P. Gong, C. Wang, H. Yu, J. Liu, C.B. Park, Carbon as a solution for nanocellular foam superinsulation, Carbon 189 (2022) 319–338, https://doi.org/10.1016/j.carbon.2021.11.041.
[33] P. Gong, P. Buahom, M.-P. Tran, M. Saniei, C.B. Park, P. Pötschke, Heat transfer in microcellular polystyrene/multi-walled carbon nanotube nanocomposite foams, Carbon 93 (2015) 819–829, https://doi.org/10.1016/j.carbon.2015.06.003.
[34] P. Gong, G. Wang, M.P. Tran, P. Buahom, S. Zhai, G. Li, C.B. Park, Advanced bimodal polystyrene/multi-walled carbon nanotube nanocomposite foams for thermal insulation, Carbon 120 (2017) 1–10, https://doi.org/10.1016/j.carbon.2017.05.029.
[35] T. Li, G. Zhao, G. Wang, L. Zhang, J. Hou, Thermal-insulation, electrical, and mechanical properties of highly-expanded PMMA/MWCNT nanocomposite foams fabricated by supercritical CO2 foaming, Macromol. Mater. Eng. 304 (2019) 1–14, https://doi.org/10.1002/mame.201800789.
[36] C.V. Vo, F. Bunge, J. Duffy, L. Hood, Advances in thermal insulation of extruded polystyrene foams, Cell. Polym. 30 (2011) 137–156, https://doi.org/10.1177/026248931103000303.
[37] Y. Li, Z. Chen, C. ZengPoly(Methyl Methacrylate) (PMMA) Nanocomposite Foams, in: Polym. Nanocomposite Foam., 2018.
[38] I. Sánchez-Calderón, V. Bernardo, J. Martín-de-León, M.Á. Rodríguez-Pérez, Thermal conductivity of low-density micro-and nanocellular poly(methyl-methacrylate) (PMMA): experimental and modeling, Mater. Des. 221 (2022) 110938, https://doi.org/10.1016/j.matdes.2022.110938.
[39] ISO 60:1977 Plastics — Determination of apparent density of material that can be poured from a specified funnel, 1977.
[40] UNE-EN 1602:2013 Thermal insulating products for building applications. Determination of the apparent density., 2013.
[41] ASTM C518 Standard Test Method for Steady-State Thermal Transmission Properties by Means of the Heat Flow Meter Apparatus, 2017.
[42] ISO 8301 Thermal insulation - Determination of steady-state thermal resistance and related properties - Heat flow meter, 1991.
[43] A. Kan, Q. Zhang, Z. Chen, J. Zhang, K. Wang, D. Cao, Novel prediction of thermal conductivities for nano-aerogel and its composites as vacuum insulation panel core, Int. J. Therm. Sci. 189 (2023) 108277, https://doi.org/10.1016/j.ijthermalsci.2023.108277.
[44] L. Glicksman, M. Schuetz, M. Sinofsky, Radiation heat transfer in foam insulation, Int. J. Heat. Mass Transf. 30 (1987) 187–197, https://doi.org/10.1016/0017-9310(87)90071-8.
[45] R.J.J. Williams, C.M. Aldao, Thermal conductivity of plastic foams, Polym. Eng. Sci. 23 (1983) 293–298, https://doi.org/10.1002/pen.760230602.
[46] S. Fantucci, A. Lorenzati, A. Capozzoli, M. Perino, Analysis of the temperature dependence of the thermal conductivity in vacuum insulation panels, Energy Build. 183 (2019) 64–74, https://doi.org/10.1016/j.enbuild.2018.10.002.
[47] R. Baetens, B.P. Jelle, J.V. Thue, M.J. Tenpierik, S. Grynning, S. Uvsløkk, A. Gustavsen, Vacuum insulation panels for building applications: a review and

beyond, Energy Build. 42 (2010) 147–172, https://doi.org/10.1016/j.enbuild.2009.09.005.
[48] K. Swimm, S. Vidi, G. Reichenauer, H.P. Ebert, Coupling of gaseous and solid thermal conduction in porous solids, J. Non Cryst. Solids 456 (2017) 114–124, https://doi.org/10.1016/j.jnoncrysol.2016.11.012.
[49] K. Swimm, G. Reichenauer, S. Vidi, H.P. Ebert, Impact of thermal coupling effects on the effective thermal conductivity of aerogels, J. Sol. -Gel Sci. Technol. 84 (2017) 466–474, https://doi.org/10.1007/s10971-017-4437-5.